Quantifying the role of the eddy transfer coefficient in simulating the response of the Southern Ocean to enhanced westerlies in a coarse-resolution model

Yiwen Li[1,2], Hailong Liu[1,2*], Zipeng Yu[1,2], Pengfei Lin[1,2] Eric Chassignet[3*], Fanghua Wu[4]

[1]State Key Laboratory of Numerical Modeling for Atmospheric Sciences and Geophysical Fluid Dynamics (LASG), Institute of Atmospheric Physics, Chinese Academy of Sciences, Beijing 100029, China

[2]College of Earth and Planetary Sciences, University of Chinese Academy of Sciences, Beijing 100049, China

[3]Center for ocean-Atmospheric Prediction Studies, Florida State University, Tallahassee 32306, Florida

[4]National Climate Center, China Meteorological Administration, Beijing 100081, China

* Corresponding author: Hailong Liu (lhl@lasg.iap.ac.cn)； Eric Chassignet (echassignet@fsu.edu)

Key Points:

- The response of the Southern Ocean to enhanced westerlies simulated with stratification-dependent eddy transfer coefficient is closest to the reference.
- The vertical variation and temporal variation in the stratification-dependent eddy transfer coefficient are the primary factors to simulating the eddy compensation.
- The eddy transfer coefficient impacts the Eulerian circulation through the density slope, changing the response of the Southern Ocean to enhanced westerlies.

Abstract

The ability of a coarse-resolution ocean model to simulate the response to enhanced westerlies in the Southern Ocean is evaluated as a function of the eddy transfer coefficient (κ) commonly used to parameterize the bolus velocities induced by unresolved eddies (Gent and McWilliams, 1990). By implementing different eddy transfer coefficients, it is shown that a coefficient κ that is stratification-dependent and varies in space and time leads to an enhanced response of the eddy-induced meridional overturning circulation (MOC), which is close to the ratio obtained from a reference eddy-resolving simulation with the same model. The compensation caused by the intensified response of the eddy-induced MOC in experiments with either constantly uniform or spatially varying eddy transfer coefficients is consistently smaller. The enhanced eddy compensation from the experiment with stratification-dependent κ can be traced to changes in the vertical derivative of κ in time. Changes in κ also affect the response of the residual Southern Ocean MOC through its Eulerian component. In the stratification-dependent case, the increased meridional gradient of κ during 1998-2007 compared to 1960-1969 decreases the meridional gradient of the density slope, which in turn dampens the meridional gradient of sea surface height and therefore leads to a weaker response of the Eulerian circulation and of the residual circulation.

Plain Language Summary

The Southern Ocean is full of mesoscale eddies with vortices on the scale of 10-100 km, which play a major role in transporting heat, salt, nutrients, and pollutants. To simulate the response of the Southern Ocean to enhanced westerlies due to global warming and ozone depletion in a coarse-resolution model, the eddy transfer coefficient is crucial, which is a key parameter in the parametrization of the mesoscale eddies. We find the stratification-dependent eddy transfer coefficient with both temporal and spatial variation has the closest simulation of the Southern Ocean response compared to the result of a high-resolution model. And it is the vertical variation and temporal variation in that scheme play the primary role in simulating the response of mesoscale eddies. There is also a secondary influence of the eddy transfer coefficient on simulating the response of the Southern Ocean by changing the density slope and corresponding meridional pressure gradient, which drives the large-scale circulation in the Southern Ocean.

1. Introduction

The circulation in the Southern Ocean is connected through the upper and lower cells of the meridional overturning circulation (MOC), along with the Antarctic Circumpolar Current (ACC). In the Southern Ocean, the upper cell of the zonal mean MOC is driven by the upwelling of North Atlantic deep waters and northward surface Ekman transport from the Southern Hemisphere westerlies (Speer et al., 2000). During the period from 1980 to 2010, the westerlies shifted poleward and intensified by ~20%, as shown by direct satellite observations and atmospheric reanalysis (Swart and Fyfe, 2012;

Bracegirdle et al., 2013; Farneti et al., 2015; Gent, 2016).

In eddy-resolving ocean models, the response of the MOC to enhanced westerlies is found to be partially compensated (~50%) by the mesoscale eddies (Marshall and Radko, 2003; Hallberg and Gnanadesikan 2006; Meredith et al., 2012; Bishop et al., 2016; Gent, 2016; Paulsen et al., 2018). In non-eddy-resolving ocean models, an increase in the zonal westerlies will only strengthen the Eulerian MOC across the ACC if a parameterization of the eddy-induced compensation is not included. This intensified Eulerian MOC then brings more water from the carbon-rich deeper ocean to the surface of the Southern Ocean, which in turn means that the ocean takes up less carbon dioxide and that the carbon dioxide in the atmosphere is overestimated in coupled models that use coarse ocean models without the parameterization of eddy compensation (Swart et al., 2014; Gent, 2016). It is therefore necessary to parameterize the eddy compensation in the ocean component of non-eddy-resolving climate ocean models.

In his review article, Gent (2016) argues that the eddy transfer coefficient commonly used to parameterize the bolus velocities induced by eddies (Gent and McWilliams, 1990, hereafter referred to as GM) must be variable in space and time to properly model the eddy compensation. His conclusion is based on the analysis of multiple non-eddy-resolving simulations with different ocean models and different expressions for the GM eddy transfer coefficient (Hofmann and Morales-Maqueda, 2011; Gent and Danabasoglu, 2011; Farneti and Gent, 2011; Farneti et al., 2015). Consequently, the impact of the eddy transfer coefficient's choice on the MOC's response could not be quantified in a consistent manner by Gent (2016).

In this paper, we quantify the eddy-induced and Eulerian MOCs' response to increased westerlies and to choices in the eddy transfer coefficient using a single non-eddy-resolving ocean model. An eddy-resolving configuration is used as the reference. In addition, we also investigate how the eddy transfer coefficient affects the Eulerian MOC as the previous studies mostly focused on the influence of eddy compensation. Specifically, we look at the impact of three widely used parametrizations of the eddy transfer coefficient. The first is the simplest and is constant in space and time (Gent and McWilliams, 1990). The second is based on the buoyancy frequency (Ferreira et al., 2005), which provides spatial and temporal variability (Danabasoglu et al., 2009). The third is dependent on eddy length and time scales provided by the eddy growth rate, the Rossby radius of deformation and the Rhines scale (Eden and Greatbatch, 2008).

The organization of the paper is as follows. In section 2, we describe the coarse and eddy-resolving ocean models, the eddy transfer coefficients, and how the MOC is decomposed into eddy-induced and mean Eulerian components. In section 3, the responses of the circulation to the intensified westerlies in the eddy-resolving model and coarse resolution experiments with different eddy transfer coefficients are discussed. Section 4 describes the influence of the eddy transfer coefficient on the eddy-induced MOC in the Southern Ocean. Section 5 reviews the impact of the eddy transfer coefficient on the Eulerian MOC. A summary and discussion of our main results are provided in the last section.

2. Models and methods

2.1 The coarse ocean model

The coarse ocean model used in this paper was developed at the State Key Laboratory of Numerical Modeling for Atmospheric Sciences and Geophysical Fluid Dynamics (LASG) through the Institute of Atmospheric Physics (IAP). The model is named the LASG/IAP Climate System Ocean Model version 3 (LICOM3), which is coupled to the Community Ice Code version 4 (CICE4) through the NCAR flux coupler version 7 (CPL7). LICOM3 has approximately 1° of horizontal resolution and 30 vertical levels. In the top 150 m, the resolution is uniform, with a grid spacing of 10 m, while the spacing is uneven below 150 m. The model used a tripole grid (Murray, 1996) with two poles in the northern hemisphere, which are located at 65°N, 30°W and 65°N, 150°E, respectively. The tidal mixing parameterization scheme of St. Laurent et al. (2012) is implemented. The coarse resolution model is a standard Coordinated Ocean-Ice Reference Experiments (CORE) II experiment, forced by the interannually varying atmospheric forcing and bulk formula developed by Large and Yeager (2009) with 6-hour interval. The experiments (hereafter referred to as LICOML) here are integrated 124 years (two 62-year CORE-II cycles), and only the second cycle is used for analysis.

2.2 The high-resolution ocean model

The high-resolution ocean model used here is the eddy-resolving version of LICOM2.0 (Liu et al., 2012), with a 0.1°×0.1° horizontal grid and 55 vertical levels. In the upper 300 m, 36 uneven levels are used, and every layer's thickness is less than 10 m. Biharmonic viscosity and diffusivity schemes are used in the momentum and tracer equations, respectively. The model domain covers 79°S-66°N, excluding the Arctic Ocean. There is a buffer zone at 66°N where temperature and salinity are restored to climatologically monthly temperature and salinity from the Levitus data (Levitus and Boyer, 1994). After the 12-year spin-up, a 60-year (1948-2007) ocean only CORE II experiment was conducted using the daily CORE forcing (Large and Yeager, 2004), which is called LICOMH hereafter. For details of the model performance, please refer to Yu et al. (2012) and Liu et al. (2014).

2.3 The eddy transfer coefficient

To evaluate the influence of different eddy transfer coefficients, five experiments have been conducted (listed in Table 1) using the coarse resolution LICOM3. The first two experiments use constant eddy transfer coefficients κ of 500 m^2s^{-1} and 1000 m^2s^{-1}, which are referred to as K500 and K1000, respectively. The next two experiments use an eddy transfer coefficient scheme based on the buoyancy frequency as described in Ferreira et al. 2005 (referred to as FMH hereafter):

$$\kappa = \frac{N^2}{N_{mld}^2}\kappa_{ref} \qquad (1)$$

where κ is the eddy transfer coefficient, κ_{ref} is constant and set to 4000 m^2s^{-1}, N^2 is the buoyancy frequency, and N^2_{mld} is the buoyancy frequency at the bottom of the mixed layer depth. The eddy transfer coefficient κ in the FMH4D experiment is computed using the instantaneous buoyancy frequency and therefore varies in space and time. In the FMH3D experiment, the eddy transfer coefficient κ is computed using the time averaged buoyancy frequency from the FMH4D experiment and therefore varies only in space.

Table 1. *Descriptions of the Experiments in This Study*

Experiment	Resolutions (°)	κ (m^2/s)	Periods
LICOMH	0.1	N/A	1949-2007
K500	1	500	1948-2009
K1000	1	1000	1948-2009
FMH3D	1	$\overline{A_I(N^2/N^2_{ref})}$	1948-2009
FMH4D	1	$A_I(N^2/N^2_{ref})$	1948-2009
EG	1	$\alpha\sigma_{x,y,z}L^2_{x,y,z}$	1948-2009

The fifth experiment uses an eddy transfer coefficient κ based on time and length scales derived from the eddy growth rate, the Rossby radius of deformation and the Rhines scale (Eden and Greatbatch, 2008). The experiment is called EG hereafter, following the abbreviation of the reference. The eddy transfer coefficient is computed as:

$$\kappa = \alpha\sigma_{x,y,z}L^2_{x,y,z} \tag{2}$$

where σ denotes an inverse eddy time scale that is given by the eddy growth rate; L is an eddy length scale, which is taken as the minimum of the local Rossby radius of deformation and the Rhines scale; and α is a constant parameter of order one (see Eden and Greatbatch (2008) and Eden et al. (2009) for details).

The corresponding eddy-induced velocity (Gent and McWilliams, 1990) is as follows:

$$u^* = (\kappa\frac{\rho_x}{\rho_z})_z = (\kappa S_x)_z \tag{3}$$

$$v^* = (\kappa\frac{\rho_y}{\rho_z})_z = (\kappa S_y)_z \tag{4}$$

where u^* and v^* are the zonal and meridional eddy-induced velocity, respectively; κ is the eddy transfer coefficient; and ρ_x, ρ_y, and ρ_z are the partial differential of density in the zonal, meridional, and vertical direction, respectively. ρ_x / ρ_z and ρ_x / ρ_z represent the zonal and meridional density slope (S_x and S_y), respectively. Because of the vertical variation of κ, the velocity can be decomposed into two terms. For the meridional velocity:

$$v^* = (\kappa S_y)_z = \kappa S_{yz} + S_y\kappa_z \tag{5}$$

where κS_{yz} represents the effect of κ on the velocity and $S_y\kappa_z$ represents the effect of the vertical variation of κ. For convenience, κS_{yz} is designated as the spatial structure term (SS) and $S_y\kappa_z$ is referred to as the vertical variation term (VV).

2.4 Decomposition of MOC from LICOMH

The residual MOC is the total MOC, which consists of both the eddy-induced MOC and the Eulerian MOC. The eddy-induced MOC in LICOMH is based on the deviation from the time-mean MOC following Poulsen et al. (2018). As in previous studies, we perform the analysis in density coordinates (e.g., Hallberg and Gnanadesikan, 2006; Munday et al., 2013; Bishop et al., 2016; Poulsen et al., 2018). The time-mean residual MOC is given by:

$$\overline{\psi}(\theta,\sigma) = \overline{\oint_0^{2\pi} \int_{\eta_B(\phi,\theta)}^{\eta(\phi,\theta,t)} v(\phi,\theta,z,t)\, dz R\cos(\theta)\, d\phi} \tag{6}$$

where ϕ,θ and z are the usual spherical coordinates, R is the Earth's radius, and σ is the potential density. η_B is the depth of the ocean bottom and $\eta(\phi,\theta,t)$ is the depth of the potential density surface, which varies in both space and time. $\overline{(\,)}$ denotes the averaging operator with respect to time.

The decomposition here can also be applied to the velocity and density field, leading to a time-mean field and its deviation. Taking the meridional velocity as an example, the decomposition is as follows:

$$v(\phi,\theta,z,t) = \overline{v}(\phi,\theta,z) + v^*(\phi,\theta,z,t) \tag{7}$$

where $\overline{v}$ is the time-mean field and v^* is the deviation. The isopycnal streamfunction derived from the time-mean field represents the Eulerian mean overturning circulation and is given by:

$$\psi(\theta,\sigma) = \oint_0^{2\pi} \int_{\eta_B(\phi,\theta)}^{\overline{\eta}(\phi,\theta)} \overline{v}(\phi,\theta,z)\, dz R\cos(\theta)\, d\phi \tag{8}$$

where $\overline{\eta}$ is the height of the time-mean density surface $\overline{\sigma}$. The difference between the time-mean residual MOC $\overline{\psi}$ and the Eulerian MOC ψ is the eddy-induced MOC:

$$\psi^* = \overline{\psi} - \psi \tag{9}$$

which captures the motion that varies on a temporal time scale shorter than the time span of the applied time-averaging operator. As in Poulsen et al. (2018), we use monthly averaged outputs to compute the eddy-induced circulation.

3. Responses to enhanced westerlies in the Southern Ocean

Studies have shown that there have been enhanced westerlies in the Southern Ocean during previous decades (Swart and Fyfe, 2012; Bracegirdle et al., 2013; Farneti et al., 2015; Gent, 2016). These enhanced westerlies are also present in the wind stress used to force the high- and low-resolution experiments. Figure 1a shows the monthly and annual running mean zonal wind stress averaged in the Southern Ocean (30-60°S and 0-360°E) for LICOML. Both curves indicate a significant increasing trend from 1948 to 2007 with a magnitude of about 0.005 N/m2 per decade. The wind stress difference between 1998-2007 and 1960-1969 (Fig. 1b) indicates that there is general enhancement of zonal wind stress in the Southern Ocean with the maximum value of 0.1 Pa. Moreover, the zonal average wind stress between 30-90°S displays a 28.9% increase of the peak value from 1998-2007 to 1960-1969. The significant multidecadal intensification of westerlies in the Southern Ocean may be driven partially by ozone depletion and global warming (Thompson and Solomon, 2002; Marshall, 2003; Miller et al., 2016). The variation of wind stress from LICOMH in the Southern Ocean is same as that of LICOML, but with a slightly weaker magnitude.

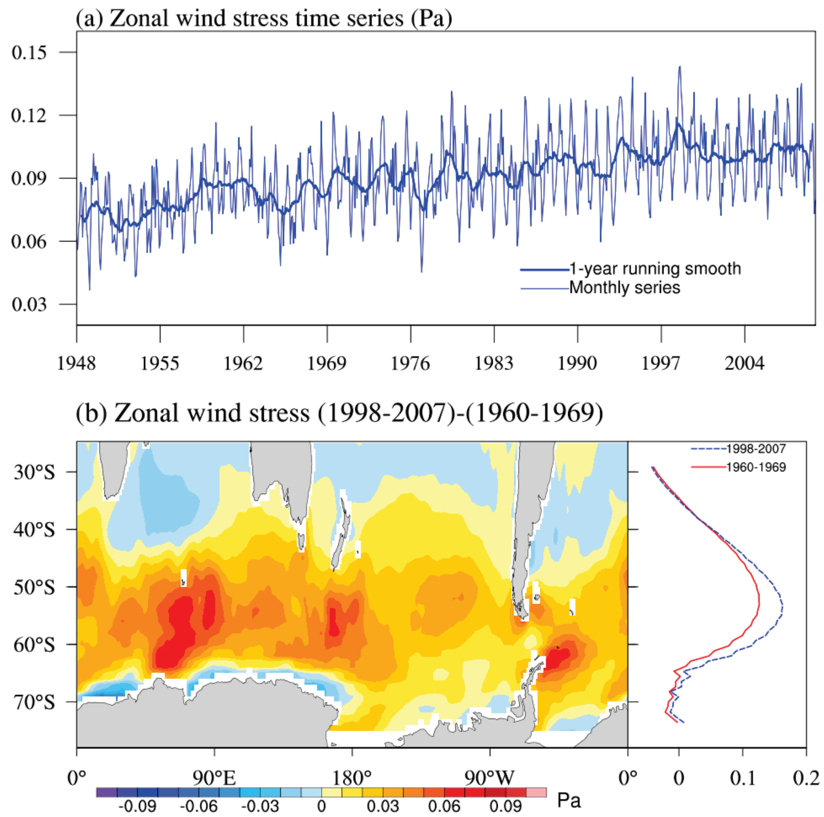

Figure 1. (a) The time series of the zonal wind stress averaged in the Southern Ocean (30°S~60°S). The thick blue line is the one-year running mean. The left panel of (b) is the differences of zonal wind stress between 1998-2007 and 1960-1969 and the right panel is the zonal mean of the zonal wind stress during 1960-1969 (red solid) and 1998-2007 (blue dash).

Because the response of the Eulerian MOC in the upper cell is compensated by eddy-induced MOC (Hallberg and Gnanadesikan 2006; Meredith and Hogg 2006; Meredith et al. 2012), eddy-resolving model outputs are necessary to quantify the eddy compensation and evaluate the coarse resolution experiments. LICOMH is used here as a reference. The top panels of Figure 2 show the residual MOC in isopycnal vertical coordinates in the Southern Ocean. The residual MOC during 1998-2007 (Fig. 2a) has an average strength of 12.05 Sv in the upper cell between 1035.0 and 1036.85 kg/m^3 and between 35°S to 60°S, while it is 5.9 Sv during 1960-1969 (Fig. 2b). There is a general about 6 Sv increase in MOC in the Southern Ocean from 1960-1969 to 1998-2007 (Fig. 2c).

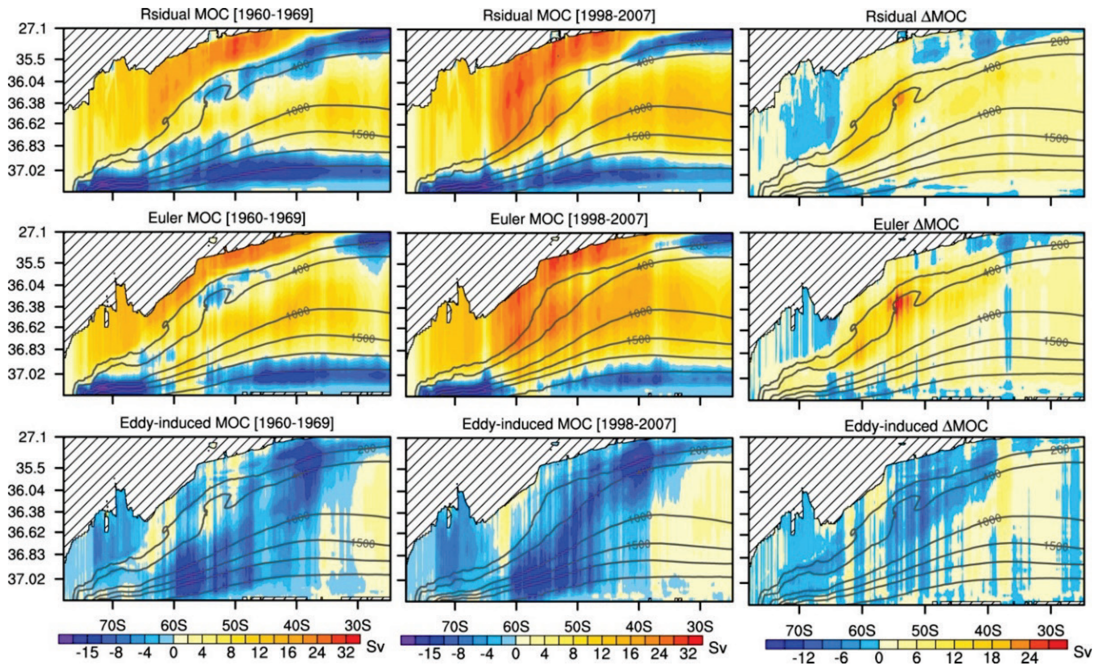

Figure 2. The top panel is the MOC of residual currents during periods of 1960-1969, 1998-2007 and their difference for LICOMH in the isopycnal coordinate, respectively. The gray lines represent the zonal averaged isobaths in isopycnal coordinates. The middle and bottom panels are same as the top one, but for the Eulerian and eddy-induced MOCs. (Unit: Sv)

For the Eulerian MOC in LICOMH, the enhancement is larger than that of the residual MOC, at a strength of 7.34 Sv (Fig. 2f). This difference between the residual and the Eulerian MOC is due to the compensation of the eddy-induced MOC, as Figure 2 shows that the circulation direction of the eddy-induced MOC (Fig. 2g, i) is opposite to that of the Eulerian MOC (Fig. 2d, e) and the eddy-induced MOC strengthens in most regions of the Southern Ocean (Fig. 2i). The strength of the oppositely directed eddy-induced MOC (referred to as eddy compensation) is 1.11 Sv, taking up to 15.1% of the response of the Eulerian MOC from 1960-1969 to 1998-2007.

For the low-resolution ocean model, the eddy transfer coefficient plays a key role in simulating the eddy compensation (Hofmann and Morales-Maqueda, 2011; Gent and Danabasoglu, 2011; Farneti and Gent, 2011; Farneti et al., 2015; Gent, 2016). It is examined in the five coarse-resolution ocean model experiments with different eddy transfer coefficients (i.e., K500, K1000, FMH3D, FMH4D, and EG). The five different eddy transfer coefficients are the constant eddy transfer coefficients (500 $m^2s^{-1}$and 1000 m^2s^{-1}), stratification dependent spatial various coefficient, stratification dependent spatiotemporal variant coefficient, and the time-length scale dependent spatiotemporal variant coefficient.

The differences of the residual MOC between 1998-2007 and 1960-1969 in all the five experiments (left panels in Fig. 3) are smaller than that of the Eulerian MOC (middle panels in Fig. 3), which is caused by the enhancement of the anti-clock wised eddy-induced MOC in all the experiments(right panels in Fig. 3).However, comparing the five experiments, the intensification of the residual MOC from FMH4D is the weakest (left panels in Fig. 3). Because the residual MOC is the sum of both the Eulerian MOC and the eddy-induced MOC, there are two factors underlying this result. On the one hand, the Eulerian MOC (middle panels in Fig. 3) shows that FMH4D and K500 have slightly weaker enhancement than other three experiments, even though all experiments exhibit similar enhancements of the Eulerian MOC. On the other hand, FMH4D has the largest enhancement and region of the anticlockwise eddy-induced MOC (right panels in Fig. 3), compared with other four experiments. Comparing differences of five experiments in the residual MOC, the Eulerian MOC and the eddy-induced MOC, the residual MOC and the eddy-induced MOC share similar feature with FMH4D having smallest clockwise circulation response to the enhanced westerlies, which implies that the response of the eddy-induced MOC makes a major contribution to the response of the residual MOC.

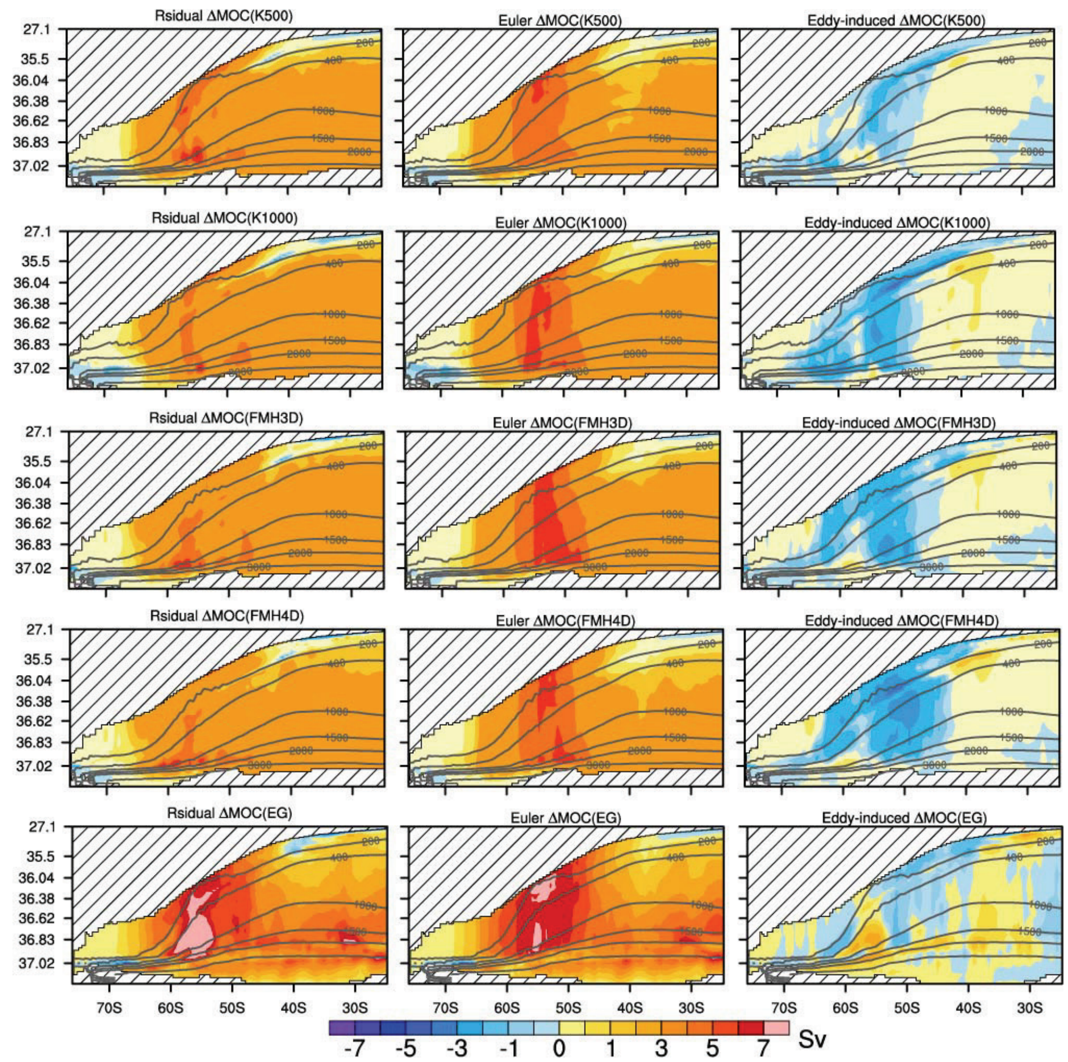

Figure 3. The top panel is the difference of the residual, Eulerian and eddy-induced MOCs between 1960-1969 and 1998-2007 for the K500 experiment. The gray lines represent the zonal averaged isobaths in isopycnal coordinates. The other panels from the second to the bottom row are for the K1000, FMH3D, FMH4D and EG experiments. (Unit: Sv)

To quantify the difference among the five experiments, the mean value in area from 1035.0 to 1036.85 kg/m^{3}and from 35°S to 60°S is defined as the strength of the upper cell. The strengths of the responses between 1960-1969 and 1998-2007 for the residual, Eulerian and eddy-induced MOC are listed in Table 2. For LICOMH, the enhanced eddy compensation is 1.11 Sv, which accounts for up to 15.1% of the change in the Eulerian MOC. Among the five coarse resolution experiments, FMH4D experiment has the largest enhanced eddy compensation of 0.63 Sv, taking up to 14.5% of the Eulerian MOC response, which is closest to the reference LICOMH, while the eddy compensations from K500, K1000, FMH3D and EG are 0.07 Sv, 0.18 Sv, 0.27 and 0.22 Sv, which take up to 1.7%, 4.1%, 5.9% and 5.5% of their Eulerian MOC response, respectively. This result indicates that both spatial and temporal variances of the eddy transfer coefficient are crucial to the eddy compensation. Furthermore, the contrast between FMH3D and FMH4D also indicates that the spatial variant eddy transfer coefficient is not enough to simulate the whole compensation effect. Compared with FMH4D, the spatial variance only makes 40.7% contribution to the eddy compensation in terms of the strength of the eddy compensation.

Table 2. *Differences of the Strength for the Residual, Eulerian and Eddy-induced MOC Between 1960-1969 and 1998-2007 Among the High-resolution Model and Five Coarse Resolution Experiments.*

Experiments	Residual	Eulerian	Eddy (Ratio)
LICOMH	6.15	7.34	1.11 (15.1%)
K500	4.12	4.19	0.07 (1.7%)
K1000	4.25	4.44	0.18 (4.1%)
FMH3D	4.33	4.59	0.27 (5.9%)
FMH4D	3.69	4.33	0.63 (14.5%)
EG	3.79	4.01	0.22 (5.5%)

Note. The strength is the mean value from 1035.0 to 1036.85 kg/m^3 and from 35°S to

60°S. The values in the bracket are the ratios of the eddy-induced MOC to the Eulerian MOC. (Unit: Sv)

Based on the comparison among the residual, Eulerian and eddy-induced circulations from five different eddy transfer coefficient experiments and LICOMH as reference, responses of the residual MOC from LICOML experiments are mainly attributed to the eddy compensation, even though the Eulerian MOC also makes contribution to it. Besides, the spatiotemporal variation of the eddy transfer coefficient, especially the temporal variation of the coefficient, is proved to be the more crucial factor in the coarse-resolution model LICOML to simulating the eddy compensation. However, how the spatiotemporal variation of the eddy transfer coefficient affects the eddy compensation and why temporal variation is more important still need more analysis.

4. Influence on the eddy compensation

As shown in Section 3, the response of the residual MOC is weaker than that of the Eulerian MOC mainly due to the intensified eddy compensation. There are two factors underlying this phenomenon. First, the eddy-induced MOC is anti-clockwise, which is opposite to the direction of the Eulerian MOC. Second, the anti-clockwise eddy-induced MOC become stronger with enhancing westerlies. We find that the eddy compensation from the FMH4D experiment is closest to the high-resolution result, while the other experiments display weaker eddy compensation. Next, we determine why the eddy transfer coefficient from the FMH4D experiment leads to stronger enhancement of anti-clockwise eddy-induced MOC.

4.1 The attribution of the eddy-induced MOC

The influence of the spatially variant eddy transfer coefficient can be decomposed into two terms that represent the effect of spatial structure (SS) and the effect of the vertical variation (VV), as detailed in section 2.3. Following the decomposition, Figure 4a and 4b show the SS term- and VV term-induced MOC from the FMH4D experiment during 1960-1969, respectively. The effects of the SS term and VV term are opposite in most regions of the upper cell, especially above 1000 m. The SS term displays a clockwise MOC above 1000 m between 40°S to 65°S, which enhances the clockwise Eulerian MOC. However, the VV term shows an anti-clockwise MOC in the region of the upper cell, which compensates the Eulerian MOC. When comparing the two terms (SS and VV) with the eddy-induced MOC, the VV term plays the major role in the eddy-induced MOC, because the sum of the two terms displays an anti-clockwise MOC in the upper cell region (Fig. 4c), which compensates the Eulerian MOC. In addition, the right panels in Figure 4 show the corresponding multidecadal response of the two terms induced MOC and their sum. The multidecadal responses exhibit intensification in the two terms induced MOC (Fig. 4d and 4e), as the SS term has a stronger clockwise MOC in the upper cell between 40°S to 60°S and the VV term has a stronger anti-clockwise MOC in all region. The sum of the two terms also displays an enhanced anti-clockwise MOC in most regions of the upper cell between 40°S to 60°S, which is in accordance with the result during 1960-1969. So, the VV term is the crucial factor leading to the eddy compensation.

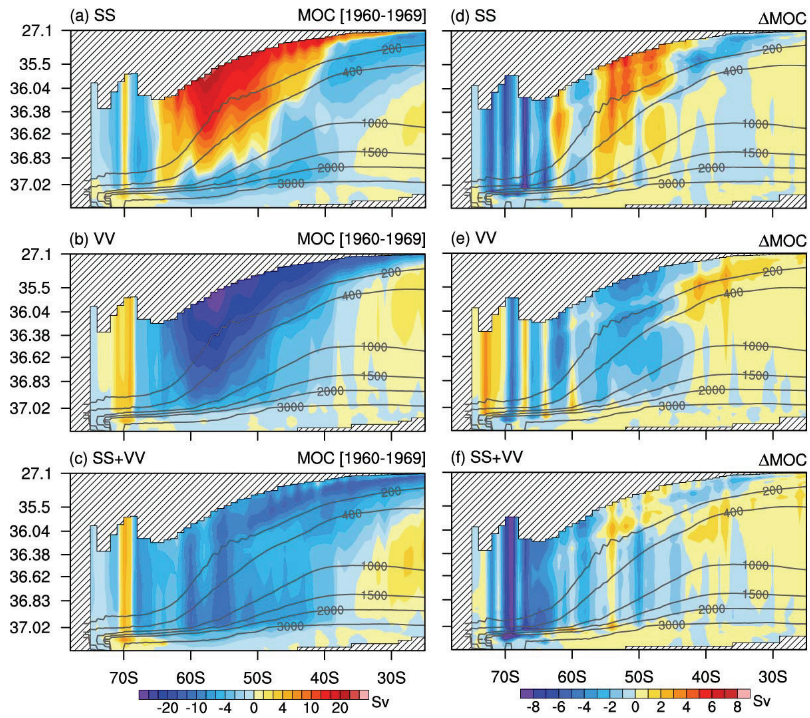

Figure 4. The left panels from top to bottom are the SS, VV components of eddy-induced MOCs, and their sum during 1960-1969. The right panels are the differences between 1960-1969 and 1998-2007. The gray lines are the zonal averaged isobaths in isopycnal coordinates during the periods. (Unit: Sv)

Even though the VV term proved to be the major contribution of the eddy compensation and its response in the FMH4D experiment, it is not clear if it is caused by the eddy transfer coefficient or the density distribution, which are the two components of VV term. The left panels in Figure 5 show the VV term-induced velocity and its two components. In terms of the circulation direction, because the vertical variation of κ (κ_z) is negative in all the regions (Fig. 5c), the sign of the VV term-induced velocity

(Fig. 5a) is subject to that of the meridional density slope (Fig. 5b). Besides, as the VV term-induced velocity is the product of the two components and κ_z barely changes under 400 m, the distribution of the VV term-induced velocity under 400 m is basically dependent on the distribution of the meridional density slope. The standard deviations of the absolute standardized κ_z and meridional density slope under 400 m are 0.39 and 0.83 respectively, which also substantiate that finding.

The role of the components in the SS term-induced velocity is different from that in the VV term-induced velocity. The circulation direction of the SS term-induced velocity (Fig. 5d) is also determined by the meridional density slope, because the sign of the eddy transfer coefficient is positive in all regions (Fig. 5f). However, the strength structure of the SS term-induced velocity is mostly dependent on the structure of the eddy transfer coefficient, rather than the vertical variation of the meridional density slope. Because the structure of the eddy transfer coefficient has a larger variation than the vertical variation of the meridional density slope, and the standard deviation of the absolute standardized vertical variation of the meridional density slope is 0.43, while that of eddy transfer coefficient is 0.80.

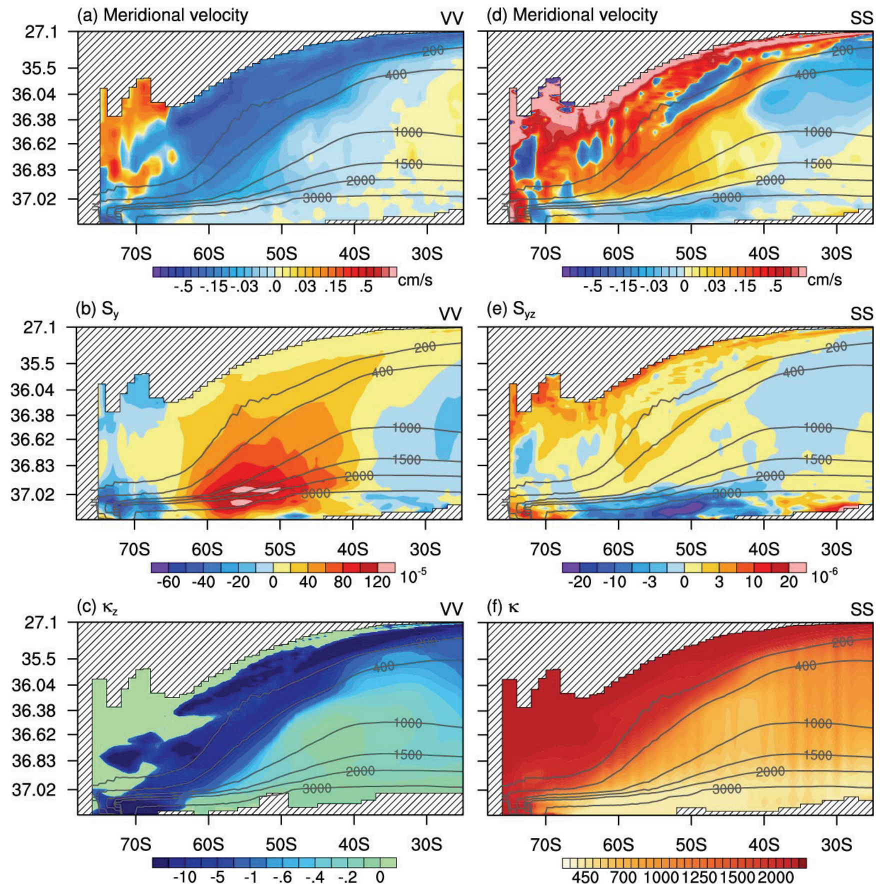

Figure 5. The left panels are the VV term-induced velocity and its two components, the meridional density slope (S_y) and the vertical variation of κ (κ_z). The right panels show the SS term-induced velocity and its two components, the vertical variation of the meridional density slope (S_{yz}) and κ. The gray lines represent the isobaths in isopycnal coordinates. The units for the velocity, S_{yz}, κ_z and κ are cm/s, m^{-1}, ms^{-1} and m^2s^{-1}, respectively.

4.2 The attribution of the response

As Figures 4d and 4e show, the responses of the VV term and SS term both have corresponding intensifications over a multidecadal scale. However, it is unclear if the multidecadal responses come from the response of eddy transfer coefficient or the response of the density slope.

The response of the VV term-induced velocity can be decomposed as follows:

$$\begin{aligned}\Delta v_{VV}^{*} &= v_{1998-2007}^{*} - v_{1960-1969}^{*} \\ &= (S + S')(\kappa_z + \kappa_z') - S\kappa_z \\ &= S'\kappa_z + S\kappa_z' + S'\kappa_z' \qquad (10)\end{aligned}$$

where Δv_{VV}^{*} is the response between 1998-2007 and 1960-1969; S and κ_z represent the meridional density slope and the vertical variation of the eddy transfer coefficient during 1960-1969, respectively; and S' and κ_z' are the responses between 1998-2007 and 1960-1969 for S and κ_z. Thus, the response of the VV term-induced velocity consists of $S'\kappa_z$, $S\kappa_z'$ and $S'\kappa_z'$. And $S'\kappa_z'$ is a second order small quantity, which means $S'\kappa_z$ and $S\kappa_z'$ are the two major factors attributed to the response. When comparing the response of the VV term-induced velocity with its two factors (Fig. 6), it is clear that $S\kappa_z'$ is the dominant factor, because the pattern and value of $S\kappa_z'$ are closer to those of the VV term-induced velocity. Even though $S'\kappa_z$ decrease the value of the response above 400 m, it doesn't change the direction or the pattern of the circulation. This result also indicates that the response of the eddy transfer coefficient makes the major contribution to the response of the VV term-induced velocity.

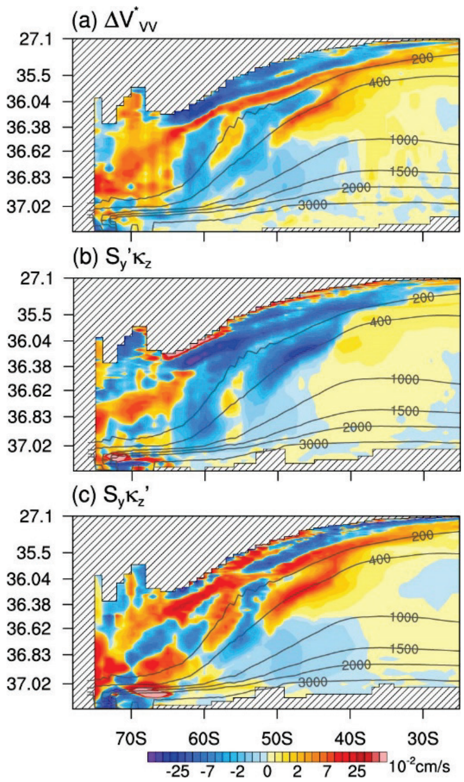

Figure 6. The top panel is the difference of the VV term-induced velocity between 1960-1969 and 1998-2007. The middle panel is the product of the difference of the meridional density slope between the two decades and the vertical variation of κ during 1960-1969. The bottom panel is the product of the meridional density slope during 1960-1969 and the difference of the vertical variation of κ between 1998-2007 and 1960-1969. The gray lines represent the isobaths in isopycnal coordinates. (Unit: cm/s)

For the SS term-induced velocity, the decomposition is as follows:

$$\begin{aligned}\Delta v_{SS}^* &= v_{1998-2007}^* - v_{1960-1969}^* \\ &= (\kappa + \kappa')(S_z + S_z') - \kappa S_z \\ &= S_z'\kappa + S_z\kappa' + S_z'\kappa' \qquad (11)\end{aligned}$$

where Δv_{SS}^* is the response between 1998-2007 and 1960-1969; S_z and κ represent the vertical variation of the meridional density slope and the eddy transfer coefficient during 1960-1969, respectively; S_z' and κ' are the responses between 1998-2007 and 1960-1969 for S_z and κ. The comparison among the SS term-induced velocity and its two factors (Fig. 7) is different from the VV term-induced velocity (Fig. 6). The response of the SS term-induced velocity does not come from the response of κ, i.e., $S_z\kappa'$. The dominant factor for the response of the SS term-induced velocity is $S_z'\kappa$, which is caused by the response of the density slope.

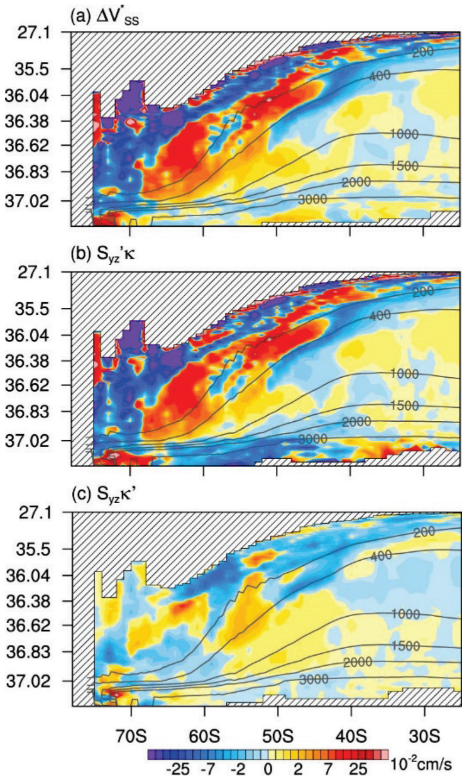

Figure 7. The top panel is the difference of the SS term-induced velocity between 1960-1969 and 1998-2007. The middle panel is the product of the difference of the vertical variation of the meridional density slope between the two decades and κ during 1960-1969. The bottom panel is the product of the vertical variation of the meridional density slope during 1960-1969 and the difference of κ from 1998-2007 to 1960-1969. The gray lines represent the isobaths in isopycnal coordinates. (Unit: cm/s)

In summary, the VV term-induced circulation enhances the compensation is because the direction of the VV term-induced circulation is dominated by the density slope and the response of it is controlled by the response of the eddy transfer coefficient. The SS term-induced circulation is not only controlled by the feature of the density slope, but also subjected to the feature of the eddy transfer coefficient. And the response of the SS term comes from the density slope rather than the eddy transfer coefficient. As the density slope exhibit the characteristic of the baroclinic instability and the response of the eddy transfer coefficient shows the stratification-dependent temporal variability, it implies that eddy parameterization should contain the features of the baroclinic instability and the temporal variability of the stratification to simulating the intensification of the eddy compensation.

5. Influence on the Eulerian circulation

Since the residual circulation is the result of the eddy-induced circulation and the Eulerian circulation, the response of the residual circulation to the intensified westerlies is not only determined by the eddy compensation but also influenced by the response of the Eulerian circulation. The Eulerian (mainly Ekman) circulation is mostly driven by wind stress and buoyancy forcing (Marshall and Speer, 2012), but also influenced by the eddy transfer coefficient indirectly. Differences of zonal mean wind stress peak between 1960-1969 and 1998-2007 from all the five experiments are 0.04Pa, but the responses of the Eulerian MOC from the EG, K500 and FMH4D experiments have the smaller value of 4.01, 4.19 and 4.33 Sv, while the responses from K1000 and FMH3D are 4.44 and 4.59 Sv, respectively (Table. 2). With the same wind stress forcing in all the five CORE-II experiments, differences among their Eulerian MOC persist, which may due to the indirect effect of the eddy transfer coefficient.

Table 3. *The Minimum and Maximum of the SSH Difference Between 1960-1969 and 1998-2007 (ΔSSH), and the Maximum Meridional Gradient of ΔSSH. (Unit: cm)*

Experiments	**Minimum of ΔSSH**	**Maximum of ΔSSH**	**Maximum gradient of ΔSSH**
K500	-5.24	7.66	12.9
K1000	-8.06	7.01	15.07
FMH3D	-8.51	6.65	15.16
FMH4D	-6.99	6.51	13.50
EG	-3.51	4.56	8.07

Because the Eulerian MOC is driven by the meridional pressure gradient caused by westerlies and the buoyancy forcing in the Southern Ocean, and the sea surface height (SSH) can reflect the meridional pressure gradient, SSH is analyzed to exhibit how eddy transfer coefficient impacts the response of the Eulerian MOC. Figure 8 displays the differences of zonal mean SSH between 1960-1969 and 1998-2007 (ΔSSH) from all five experiments. There is an obvious enhancement in their meridional gradient, since SSH increases between 45°S and 30°S and decreases at the south of 45°S. However, Table 3 shows the differences among the five experiments in regard to the details. The minimum of ΔSSH in the EG, K500 and FMH4D experiments is larger than other two experiments and the maximum of ΔSSH is smaller, which leads to smaller meridional ΔSSH gradients in the EG, K500 and FMH4D experiments. That smaller meridional ΔSSH gradient means a smaller intensified meridional pressure gradient, which is in accordance with the response strengths of the Eulerian MOC.

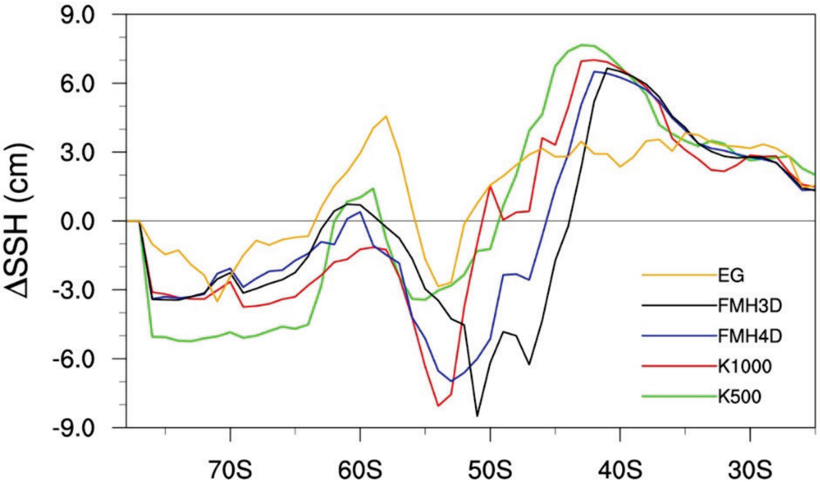

Figure 8. The differences between 1960-1969 and 1998-2007 of the zonal-averaged SSH (ΔSSH). The zonal average is first applied to the positive and negative differences, respectively; then the sum of zonal-averaged positive and negative differences is the ΔSSH, avoiding the off-set of the positive and negative anomalies in the same latitude. The orange, black, blue, red, and green lines represent the results for the EG, FMH3D, FMH4D, K1000, and K500 experiments, respectively. (Unit: cm)

Since SSH has a corresponding relationship with the thermocline in the tropic Pacific due to the wind-driven circulation, it is reasonable to consider the influence of the density distribution on SSH in the Southern Ocean. Figure 9 shows the differences of zonal mean 1037.06 kg/m^3 depth between 1960-1969 and 1998-2007 (denoted by $\Delta D_{37.06}$) in all the five experiments. It also exhibits a similar intensified meridional gradient, as the 1037.06 kg/m^3 isopycnal decreases near 70°S, but increases at the northern region of the Southern Ocean. For the differences among the five experiments (Table. 4), the meridional density gradient is not consistent with the ΔSSH gradient, which should agree with ΔSSH if the Eulerian circulation is totally wind-driven. That inconsistence implies the density slope also make contribution the response of the Eulerian circulation, as the maximal meridional gradient of $\Delta D_{37.06}$ in FMH4D experiment is smallest, which decreases the response of the meridional pressure gradient and the enhancement of the Eulerian MOC.

Table 4. *The Minimum and Maximum of the Difference of 1037.06 kg/m^3 Depth Between 1960-1969 and 1998-2007 (ΔD), and the Maximum Meridional Gradient of ΔD. (Unit: m)*

Experiments	**Minimum of ΔD**	**Maximum of ΔD**	**Maximum gradient of ΔD**
K500	-215.87	229.40	445.27
K1000	-203.29	142.20	345.49
FMH3D	-418.85	270.43	689.28
FMH4D	-68.75	264.62	333.37
EG	-1254.76	355.65	1610.41

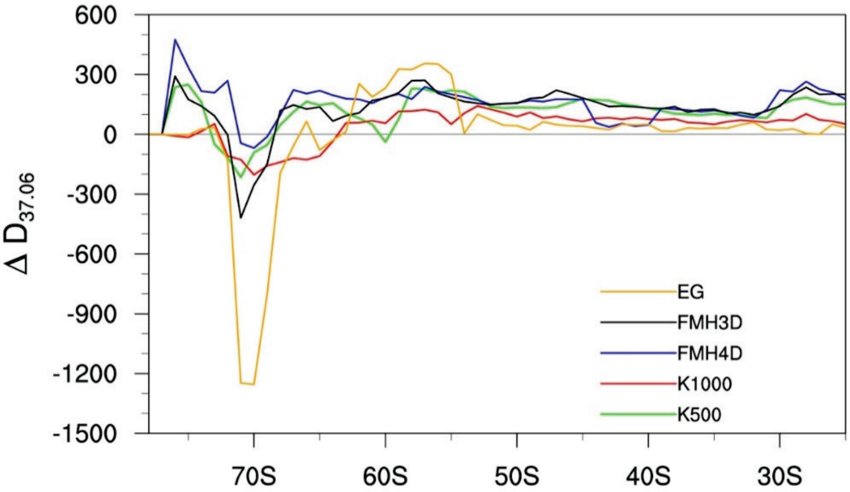

Figure 9. The differences of the zonal-averaged 1037.06 kg/m^3 depth between 1960-1969 and 1998-2007, and the zonal average is same as that in Figure 8. The orange, black, blue, red, and green lines represent the results for the EG, FMH3D, FMH4D, K1000, and K500 experiments, respectively. (Unit: m)

That relationship among the Eulerian MOC, SSH and density in the FMH4D experiment suggests that the eddy transfer coefficient impacts the Eulerian MOC through the density, which is affected by the eddy-induced heat and salinity advection dominated by the eddy transfer coefficient. Figure 10 shows the zonal mean density distribution from the K500 and K1000 experiments during the same period from 1960-1969, which indicates that larger values of eddy transfer coefficient can slump the density slope in the meridional direction and decrease the meridional gradient, as the density decreases in the south and increases in the north. Therefore, after the same period, the decrease of the meridional density gradient from the K1000 experiment is larger than that from the K500 experiment, which leads to a smaller enhancement of the meridional density gradient.

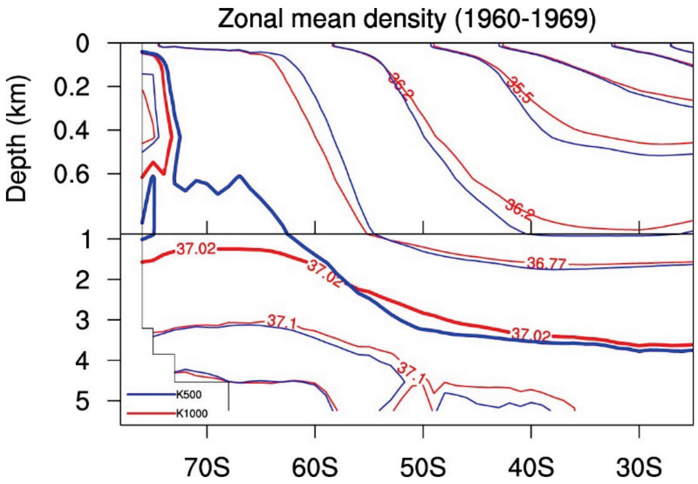

Figure 10. The zonal mean density layers during 1960-1969. The blue lines represent the K500 experiment and the red lines represent the K1000 experiment.

For the FMH3D experiment, it has a smaller value than the K500 experiment under 1000 m (Fig. 11a), which leads to a smaller decrease in the meridional density gradient. That distribution of the eddy transfer coefficient leads to a greater intensification of the meridional density gradient in the FMH3D experiment than that in the K500 experiment. However, for the FMH4D experiment, there is an obvious increase of eddy transfer coefficient near the northern pycnocline over time (Fig. 11b), while the eddy transfer coefficient barely changes in the south. The larger eddy transfer coefficient in the north lifts the density slope, leading to a smaller meridional density gradient than that in the FMH3D experiment.

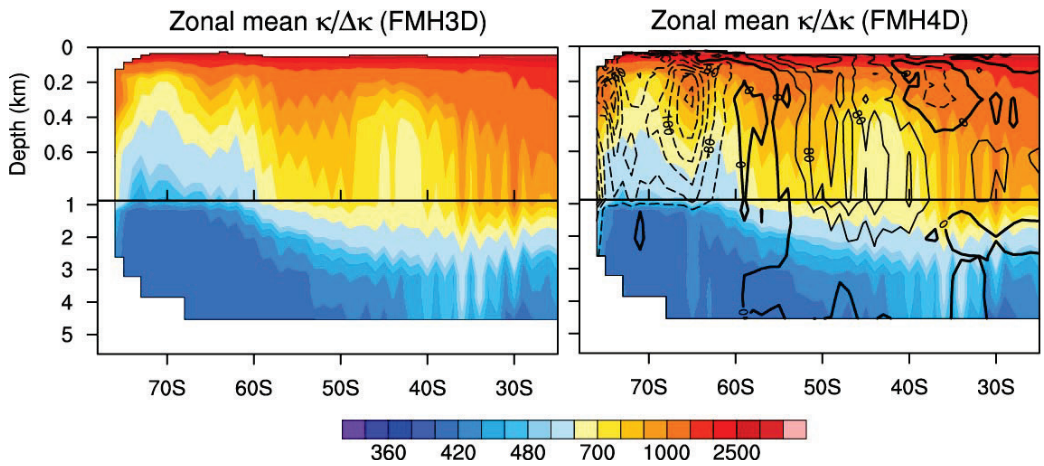

Figure 11. The left panel is the zonal mean eddy transfer coefficient in the FMH3D experiment. The shaded area in the right panel is the zonal mean eddy transfer coefficient in the FMH4D experiment and the contours are the difference between 1960-1969 and 1998-2007. The solid lines represent positive anomaly and the dashed lines represent negative anomaly. (Unit: m^2s^{-1})

Above all, the larger value of the eddy transfer coefficient and its increase with time in the FMH4D experiment leads to the weakest meridional density gradient among the five experiments. The corresponding weakest response of the SSH meridional gradient makes the response of the Eulerian MOC in the FMH4D experiment the weakest.

6. Discussion and Summary

By comparing several coarse resolution ocean models forced by the CORE-II atmospheric fields, Downes et al. (2018) showed that the Southern Ocean MOC decadal trends are controlled by changes in surface buoyancy fluxes and the choice of eddy parameterization. Furthermore, Gent (2016) surmised that a spatially and temporally varying eddy transfer coefficient in the GM parametrization is necessary to simulate the response of the Southern Ocean to enhanced westerlies in non-eddy-resolving ocean models. In this study, we quantify the influence of five eddy transfer coefficients on the response of Southern Ocean MOCs to intensified westerlies in one non-eddy-resolving ocean model driven by CORE-II forcing. We show that the experiment with a spatially and temporally varying coefficient based on the buoyancy frequency has the closest Southern Ocean MOC response when compared to the eddy-resolving numerical simulation used as a reference. A spatial and temporal variability in κ leads to stronger eddy compensation and a weaker enhancement of the Eulerian MOC, with both the eddy-induced and Eulerian MOC contributing to the residual MOC.

To quantify the impact of the eddy transfer coefficient's spatial and temporal variability, the ratio between the responses of eddy-induced MOC and Eulerian MOC from the five experiments are computed. The constant eddy transfer coefficient cases (K500 and K1000) have ratios of 1.7% and 4.1%, respectively, while that the ratio for the spatially variant (FMH3D) and spatio-temporally variant (FMH4D) cases are 5.9% and 14.5%, respectively. This finding implies that the spatial variation in κ plays an indispensable role in the eddy compensation and that the temporal variability is even more efficient in simulating the response of eddy compensation in the Southern Ocean. This is because the influence of spatial variability takes up 40.7% of the total contribution versus 59.3% for the temporal variability.

By decomposing the eddy-induced MOC into the VV and SS terms, which are based on the vertical variation of the eddy transfer coefficient and the spatial structure of the coefficient, respectively, the eddy compensation from the FMH4D experiment with the stratification-dependent eddy transfer coefficient can be traced to changes in the vertical derivative of the coefficient rather than its spatial structure. A further decomposition of the response of the VV term-induced MOC from the FMH4D experiment is conducted. It shows the intensified VV term's eddy compensation is primarily attributed to the response of the eddy transfer coefficient, which also emphasizes the role of the temporal variability of the coefficient.

Additionally, the eddy transfer coefficient also influences the response of the Southern Ocean residual MOC through its Eulerian component. In the FMH4D experiment, the increased meridional gradient of κ during the 1998-2007 period over 1960-1969 decreases the meridional gradient of the density slope. Consequently, the meridional SSH gradient also decreases, leading to a weaker response of the Eulerian circulation.

The present results show that a stratification-based parameterization that allows for spatial and temporal variability in the eddy-induced MOC is a good option for effectively simulating the response of the Southern Ocean circulation to climate change in coarse ocean models. Even though the Southern Ocean circulation response in the FMH4D experiment is close to that of the high-resolution ocean model, it is unclear how the strong anisotropy in the Southern Ocean should be taken into account when deriving the eddy transfer coefficient (Gent and Smith, 2004; Abernathey et al., 2013). Additional research on how anisotropy in the eddy transfer coefficient would affect the Southern Ocean circulation response is needed.

Acknowledgements

Drs. Li, Liu, Lin and Mr. Yu are supported by National Key R&D Program for Developing Basic Sciences (2016YFC1401401, 2016YFC1401601), and the National Natural Science Foundation of China (Grants 41576025, 41576026, 41776030, and 41931183). Dr. Chassignet is supported by the CAS President's International Fellowship Initiative (PIFI) for 2019 and grant???. The data used in this paper can be downloaded from https://osf.io/nr4yf/.

References

Abernathey, R. P., & Marshall, J. (2013). Global surface eddy diffusivities derived from satellite altimetry. Journal of Geophysical Research: Oceans, 118(2), 901-916. https://doi.org/10.1002/jgrc.20066

Bishop, S. P., Gent, P. R., Bryan, F. O., Thompson, A. F., Long, M. C., & Abernathey, R. (2016). Southern Ocean overturning compensation in an eddy-resolving climate simulation. Journal of Physical Oceanography, 46(5), 1575-1592. https://doi.org/10.1175/JPO-D-15-0177.1

Bracegirdle, T. J., Shuckburgh, E., Sallee, J. B., Wang, Z., Meijers, A. J., Bruneau, N., ... & Wilcox, L. J. (2013). Assessment of surface winds over the Atlantic, Indian, and Pacific Ocean sectors of the Southern Ocean in CMIP5 models: Historical bias, forcing response, and state dependence. Journal of Geophysical Research: Atmospheres, 118(2), 547-562. https://doi.org/10.1002/jgrd.50153

Downes, S. M., Spence, P., & Hogg, A. M. (2018). Understanding variability of the Southern Ocean overturning circulation in CORE-II models. Ocean Modelling, 123, 98-109. https://doi.org/10.1016/j.ocemod.2018.01.005

Eden, C., Jochum, M., & Danabasoglu, G. (2009). Effects of different closures for thickness diffusivity. Ocean Modelling, 26(1-2), 47-59. https://doi.org/10.1016/j.ocemod.2008.08.004

Eden, C., & Greatbatch, R. J. (2008). Towards a mesoscale eddy closure. Ocean Modelling, 20(3), 223-239. https://doi.org/10.1016/j.ocemod.2007.09.002

Eden, C., Jochum, M., & Danabasoglu, G. (2009). Effects of different closures for thickness diffusivity. Ocean Modelling, 26(1-2), 47-59. https://doi.org/10.1016/j.ocemod.2008.08.004

Farneti, R., & Gent, P. R. (2011). The effects of the eddy-induced advection coefficient in a coarse-resolution coupled climate model. Ocean Modelling, 39(1-2), 135-145. https://doi.org/10.1016/j.ocemod.2011.02.005

Farneti, R., Downes, S. M., Griffies, S. M., Marsland, S. J., Behrens, E., Bentsen, M., ... & Canuto, V. M. (2015). An assessment of Antarctic Circumpolar Current and Southern Ocean meridional overturning circulation during 1958–2007 in a suite of interannual CORE-II simulations. Ocean Modelling, 93, 84-120. https://doi.org/10.1016/j.ocemod.2015.07.009

Ferreira, D., Marshall, J., & Heimbach, P. (2005). Estimating eddy stresses by fitting dynamics to observations using a residual-mean ocean circulation model and its adjoint. Journal of Physical Oceanography, 35(10), 1891-1910. https://doi.org/10.1175/JPO2785.1

Gent, P. R. (2016). Effects of Southern Hemisphere wind changes on the meridional overturning circulation in ocean models. Annual review of marine science, 8, 79-94. https://doi.org/10.1146/annurev-marine-122414-033929

Gent, P. R., & Danabasoglu, G. (2011). Response to increasing Southern Hemisphere winds in CCSM4. Journal of climate, 24(19), 4992-4998. https://doi.org/10.1175/JCLI-D-10-05011.1

Gent, P. R., & Mcwilliams, J. C. (1990). Isopycnal mixing in ocean circulation models. Journal of Physical Oceanography, 20(1), 150-155. https://doi.org/10.1175/1520-0485(1990)020<0150:IMIOCM>2.0.CO;2

Hallberg, R., & Gnanadesikan, A. (2006). The role of eddies in determining the structure and response of the wind-driven Southern Hemisphere overturning: Results from the Modeling Eddies in the Southern Ocean (MESO) project. Journal of Physical Oceanography, 36(12), 2232-2252. https://doi.org/10.1175/JPO2980.1

Hofmann, M., & Morales Maqueda, M. A. (2011). The response of Southern Ocean eddies to increased midlatitude westerlies: A non-eddy resolving model study. Geophysical Research Letters, 38(3). https://doi.org/10.1029/2002GL015919

Large, W. G., & Yeager, S. G. (2004). Diurnal to decadal global forcing for ocean and sea-ice models: the data sets and flux climatologies. NCAR Technical Note. National Center for Atmospheric Research, 11, 324-336. https://doi.org/10.5065/D6KK98Q6

Large, W. G., & Yeager, S. G. (2009). The global climatology of an interannually varying air–sea flux data set. Climate dynamics, 33(2-3), 341-364. https://doi.org/10.1007/s00382-008-0441-3

Levitus, S., and T. P. Boyer (1994), World Ocean Atlas 1994, vol. 4, Temperature, NOAA Atlas NESDIS 4, 129 pp., Natl. Oceanic and Atmos. Admin., Silver Spring, Md.

Liu, H., Lin, P., Yu, Y., & Zhang, X. (2012). The baseline evaluation of LASG/IAP climate system ocean model (LICOM) version 2. Acta Meteorologica Sinica, 26(3), 318-329. https://doi.org/10.1007/s13351-012-0305-y

Liu, H., Yu, Y., Lin, P., & Wang, F. (2014). High-resolution LICOM. In Flexible Global Ocean-Atmosphere-Land System Model (pp. 321-331). Springer, Berlin, Heidelberg. https://doi.org/10.1007/978-3-642-41801-3_38

Marshall, G. J. (2003). Trends in the Southern Annular Mode from observations and reanalyses. Journal of Climate, 16(24), 4134-4143. https://doi.org/10.1175/1520-0442(2003)016<4134:TITSAM>2.0.CO;2

Marshall, J., & Radko, T. (2003). Residual-mean solutions for the Antarctic

Circumpolar Current and its associated overturning circulation. Journal of Physical Oceanography, 33(11), 2341-2354. https://doi.org/10.1175/1520-0485(2003)033<2341:RSFTAC>2.0.CO;2

Marshall, J., & Speer, K. (2012). Closure of the meridional overturning circulation through Southern Ocean upwelling. Nature Geoscience, 5(3), 171. https://doi.org/10.1038/ngeo1391

Meredith, M. P., & Hogg, A. M. (2006). Circumpolar response of Southern Ocean eddy activity to a change in the Southern Annular Mode. Geophysical Research Letters, 33(16). https://doi.org/10.1029/2006GL026499

Meredith, M. P., Naveira Garabato, A. C., Hogg, A. M., & Farneti, R. (2012). Sensitivity of the overturning circulation in the Southern Ocean to decadal changes in wind forcing. Journal of Climate, 25(1), 99-110. https://doi.org/10.1175/2011JCLI4204.1

Miller, R. L., Schmidt, G. A., & Shindell, D. T. (2006). Forced annular variations in the 20th century intergovernmental panel on climate change fourth assessment report models. Journal of Geophysical Research: Atmospheres, 111(D18). doi:10.1029/2005JD006323

Munday, D. R., Johnson, H. L., & Marshall, D. P. (2013). Eddy saturation of equilibrated circumpolar currents. Journal of Physical Oceanography, 43(3), 507-532. https://doi.org/10.1175/JPO-D-12-095.1

Murray, R. J. (1996). Explicit generation of orthogonal grids for ocean models. Journal of Computational Physics, 126(2), 251-273.

https://doi.org/10.1006/jcph.1996.0136

Poulsen, M. B., Jochum, M., & Nuterman, R. (2018). Parameterized and resolved Southern Ocean eddy compensation. Ocean Modelling, 124, 1-15. https://doi.org/10.1016/j.ocemod.2018.01.008

Smith, R. D., & Gent, P. R. (2004). Anisotropic Gent–McWilliams parameterization for ocean models. Journal of Physical Oceanography, 34(11), 2541-2564. https://doi.org/10.1175/JPO2613.1

Speer, K., Rintoul, S. R., & Sloyan, B. (2000). The diabatic Deacon cell. Journal of physical oceanography, 30(12), 3212-3222. https://doi.org/10.1175/1520-0485(2000)030<3212:TDDC>2.0.CO;2

St. Laurent, L. C., Simmons, H. L., & Jayne, S. R. (2002). Estimating tidally driven mixing in the deep ocean. Geophysical Research Letters, 29(23), 21-1. https://doi.org/10.1029/2002GL015633

Swart, N. C., & Fyfe, J. C. (2012). Observed and simulated changes in the Southern Hemisphere surface westerly wind-stress. Geophysical Research Letters, 39(16). https://doi.org/10.1029/2012GL052810

Swart, N. C., Fyfe, J. C., Saenko, O. A., & Eby, M. (2014). Wind-driven changes in the ocean carbon sink. Biogeosciences, 11(21), 6107-6117. DOI: 10.5194/bg-11-6107-2014

Thompson, D. W., & Solomon, S. (2002). Interpretation of recent Southern Hemisphere climate change. Science, 296(5569), 895-899. DOI: 10.1126/science.1069270

Yu, Y., Liu, H., & Lin, P. (2012). A quasi-global 1/10 eddy-resolving ocean general circulation model and its preliminary results. Chinese Science Bulletin, 57(30), 3908-3916. https://doi.org/10.1007/s11434-012-5234-8